

GA-A24826

ADVANCED CONTROL TECHNIQUES AND HIGH PERFORMANCE DISCHARGES ON DIII-D

by

A.G. KELLMAN for the DIII-D TEAM

SEPTEMBER 2004



DISCLAIMER

This report was prepared as an account of work sponsored by an agency of the United States Government. Neither the United States Government nor any agency thereof, nor any of their employees, makes any warranty, express or implied, or assumes any legal liability or responsibility for the accuracy, completeness, or usefulness of any information, apparatus, product, or process disclosed, or represents that its use would not infringe privately owned rights. Reference herein to any specific commercial product, process, or service by trade name, trademark, manufacturer, or otherwise, does not necessarily constitute or imply its endorsement, recommendation, or favoring by the United States Government or any agency thereof. The views and opinions of authors expressed herein do not necessarily state or reflect those of the United States Government or any agency thereof.

GA-A24826

ADVANCED CONTROL TECHNIQUES AND HIGH PERFORMANCE DISCHARGES ON DIII-D

by

A.G. KELLMAN for the DIII-D TEAM

This is a preprint of an invited paper to be presented at the 16th ANS Topical Meeting on the Technology of Fusion Energy, Madison, Wisconsin, September 14-16, 2004 and to be printed in Fusion Science and Technology.

Work supported by
the U.S. Department of Energy
under DE-FC02-04ER54698

GENERAL ATOMICS PROJECT 30200
SEPTEMBER 2004



ADVANCED CONTROL TECHNIQUES AND HIGH PERFORMANCE DISCHARGES ON DIII-D

A.G. Kellman for the DIII-D Team

General Atomics, P.O. Box 85608, San Diego California 92186-5608, Arnie.Kellman@gat.com

The advancement of plasma control techniques has enabled significant progress to be made toward the scientific understanding and realization of Advanced Tokamak operation on DIII-D. The Advanced Tokamak features fully non-inductive current drive, operation at high plasma pressure and high energy confinement time. These features require efficient current drive systems, simultaneous control of plasma current and pressure profiles, and active feedback control of plasma instabilities. A number of key systems on DIII-D have been developed to provide this control capability. A versatile electron cyclotron heating and current drive system is routinely providing in excess of 2 MW of power for pulse lengths from 2 to 5 s. This system has been used to provide off-axis current drive, direct electron heating and pressure profile modification, and stabilization of the Neoclassical Tearing Mode instability. A combination of control of magnetic error fields, neutral beam induced plasma rotation, and active feedback stabilization using both external and internal non-axisymmetric coil systems has been used to stabilize the Resistive Wall Mode at high values of plasma pressure. Control of the ELM instability has recently been demonstrated using the newly installed internal coil system. The higher speed and expanded real-time diagnostic capability of our recently upgraded plasma control system permits these various control techniques to be simultaneously integrated to achieve our high performance discharges. This has resulted in fully non-inductively driven plasmas with $\beta_N = 3.5$ and $\beta_T = 3.6\%$ sustained for up to 1 s. Upgrades and facility modifications to further enhance our control and scientific capabilities including rotation of a neutral beamline, expanded EC system power, and installation of a new lower divertor are discussed.

I. INTRODUCTION

The goal of the DIII-D advanced tokamak program is to provide the scientific basis for the optimization of the tokamak approach to fusion energy. Design of a conventional tokamak is focussed around moderate values of plasma confinement, $H < 2$ ($H = \tau_E / \tau_{ITER89P}$) [1], and plasma stability, $\beta_N < 2.5\%$ m•Tesla/Amp [$\beta_N = \beta(I/aB)$] with high power rf and/or neutral beams proposed to achieve steady state operation. To enhance the attractiveness of the tokamak relative to a conventional

design, the DIII-D program is focusing on advancing on three key areas: high fusion power density, low current drive power requirements, and high fusion gain. To increase the fusion power density in a tokamak requires operation at higher values of root mean square β denoted as β^* [$\beta^* = 2\mu_0(\int p^2 dV)^{1/2}/B_0^2$] and thus drives the need for an effective feedback system for operating near or above conventional beta limits. To achieve steady-state operation with low circulating power drives us toward non-inductive current drive operation with a high self-generated bootstrap current fraction to reduce the power requirements for the current drive system. This again pushes operation toward high pressure since the bootstrap current fraction is approximately proportional to $\beta_N q$, where q is the safety factor. Finally, to maximize fusion gain in a compact device requires improved energy confinement in high beta discharges. A figure of merit that is often used to characterize progress toward these goals is the product of $\beta_N H$. Experiment and theory both show that the β limits are maximized by strong shaping (high triangularity and elongation) and broad pressure profiles [2,3,4]. With both optimal profiles and strong shaping, the gain in all the relevant fusion performance parameters is dramatic and both β and β^* can be increased by a factor of five [2]. Combining these requirements, results in an Advanced Tokamak (AT) that is a compact, highly shaped plasma operating at higher β_N (approaching 5), higher confinement (H approaching 3), with 100% non-inductive current drive, and high bootstrap current fraction (50–100%). To achieve these parameters requires a high degree of active control, not only of global parameters, but also of internal profiles. Plasma stability, particle and energy transport, all depend strongly on the internal profiles of current, pressure, electric field, and toroidal rotation, so that advanced control methods need to be developed. In addition, simultaneous control of these elements requires a unified control system that fully integrates all the individual control elements including the complex coupling of these different parameters.

Section II of this paper will discuss how the recent advances in plasma control techniques and capabilities on DIII-D have permitted significant progress toward this goal of an advanced tokamak. The electron cyclotron system [5,6] power and reliability have been increased and it is now used for current drive and current profile control

[7], multipoint T_e control [8], and stabilization of the Neoclassical Tearing mode instability [9]. The Resistive Wall Mode (RWM) instability at high β has been stabilized by a variety of techniques including error field correction combined with neutral beam induced rotation [10], and active feedback control using both internal [11] and external coil sets [12,13]. Progress toward combining these elements into fully integrated high performance discharges has produced a fully non-inductively driven current discharge operating at $\beta_N \sim 3.5$, above the conventional tokamak stability limit for more than four energy confinement times [7]. Two successful techniques for suppressing the pulsed heat loads associated with the Edge Localized Modes (ELMs) in H-mode discharges {Quiescent Double Barrier Mode (QDB) [14,15] and creation of a stochastic edge [16]} and the development of a technique for mitigation of disruptions of high performance plasmas (massive gas puff injection [17]) have provided possible solutions to serious engineering problems of future high power devices. The completed upgrade of the plasma control system has enabled these more sophisticated control techniques to be realized [8,18]. Future upgrades to DIII-D systems, including the expansion of the EC system, rotation of a neutral beamline from the co to counter- I_p direction to provide control of momentum input, and a new divertor structure to better pump our highest performance AT discharges will be discussed in Section III.

II. RECENT PROGRESS

The Electron Cyclotron Heating (ECH) and Current Drive (ECCD) system is a critical tool for achieving Advanced Tokamak performance on DIII-D. As the reliability and power have increased, the system has demonstrated its flexibility to address a wide range of the central control elements needed for fully integrated advanced performance discharges: current drive, current profile control, electron temperature profile and transport control, and mode stabilization. The present 110 GHz gyrotron system on DIII-D [5,6] comprises six gyrotrons in the 1 MW class, with a total source power of 5.25 MW. Three gyrotrons manufactured by CPI [19] have demonstrated 1 MW output power for 5 s and the other three manufactured by Gycom [20] have generated 0.75 MW for 2 s. The Gycom tubes utilize boron nitride windows that absorb 4% of the transmitted rf and when combined with the phase correction and focusing mirrors yield a system coupling efficiency of $\sim 85\%$. The newer CPI gyrotrons employ a high thermal conductivity diamond window that absorbs very little power and permits 10 s operation for a 1 MW beam. Earlier problems associated with contamination of the diamond window during the Au/Cu braze

process are now well understood [21] and window problems are no longer an operational issue for these gyrotrons. For the Gaussian rf beams generated by these CPI gyrotrons only one focusing mirror is required and the coupling efficiency is between 93%–95%. The gyrotrons are located ~ 100 m from the DIII-D tokamak and the rf is transmitted via evacuated circular corrugated waveguide 31.75 mm in diameter. Polarization control is provided by pairs of grooved mirrors integrated in 90° water cooled miter bends. The measured loss in the complete transmission line with 10 miter bends is approximately 20%. The final element in the system is the launcher that is located behind the vessel wall above the plasma midplane. Each launcher is independently steerable in both the poloidal and toroidal directions. This permits full coverage of the upper poloidal plane for both central and off-axis application and the $\pm 20^\circ$ toroidal scan provides capability for either co- or counter-current drive or heating. The launcher mirrors provide a narrow radial deposition width of 3–4 cm to the half power point. Because of the low loss of the entire system, the small footprint in the vessel, the ability to remotely locate the sources, and the ability to accurately steer and achieve narrow absorption of the EC power, this system is extremely well suited for use in future reactor systems.

One of the first applications for which the EC system is uniquely suited is the stabilization of the neoclassical tearing mode (NTM). The instability occurs at moderate to high beta values and can be stabilized by the ECCD replacement of “missing” bootstrap current in the unstable island. Figure 1 shows the successful stabilization of a

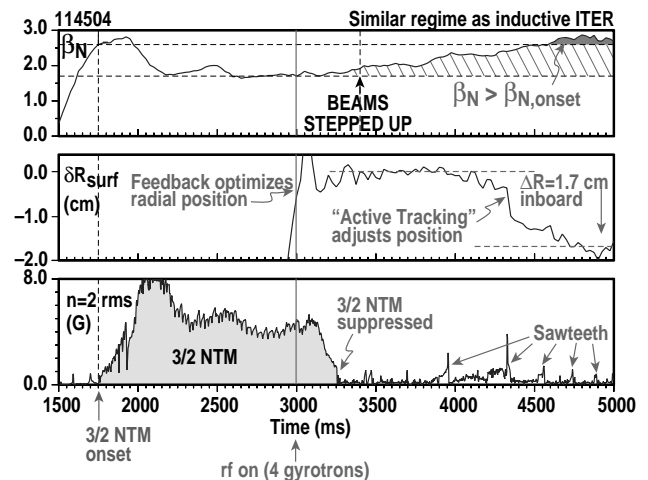


Fig. 1. Alignment of the ECCD on the $q = 3/2$ rational surface is done by the “search and suppress” algorithm in the presence of the mode and by an adaptive network predictor without the mode. (a) β_N , (b) change in plasma major radius R_{surf} , (c) $n = 2$ Mirnov amplitude.

$m = 3, n = 2$ NTM using 2.3 MW of ECCD and a control algorithm referred to as “Search and Suppress” [9]. Upon initiation of the ECCD, the plasma major radius R_{surf} is adjusted to align the island with the ECCD resonance to achieve complete mode suppression. After suppression, control is passed to an “Active Tracking” algorithm that maintains alignment by predicting the outward radial shift of the island location as the plasma beta is increased further. In the particular example shown in Fig. 1, the plasma beta is increased beyond its initial value at mode onset and alignment is maintained by the adjustment of R_{surf} of 1.7 cm after full stabilization of the mode. Two techniques have been used successfully for this active tracking. Prior to the 2004 run campaign, the tracking algorithm made use of a neural network predictor to estimate the deviations from alignment after the mode was suppressed. Recently, the real-time equilibrium reconstruction algorithm (RTEFIT) [22] has been upgraded to provide a real-time safety factor (q) calculation based on the motional Stark effect (MSE) diagnostic combined with magnetic measurements. Since the NTM island resides on the corresponding resonant flux surface with safety factor given by the m/n ratio, the Active Tracking algorithm maintains alignment with the $3/2$ surface. In addition, by applying the ECCD early, i.e., before the onset of the NTM, this tracking algorithm can avoid the initiation of the mode and allow higher stable beta without the NTM ever appearing. Similar stabilization has also been achieved of the more dangerous $m = 2/n = 1$ NTM that typically leads to disruption [23]. Planned upgrades include increases in the EC system power to allow simultaneous control of both the $3/2$ and $2/1$ tearing modes and real-time mirror steering to provide accurate localization of the ECCD with fixed discharge shape and position.

In another application of the EC system for mode control, the ECCD was applied to modify the current profile and provide a q profile that is stable to NTMs. In one particular example, the application of ECCD was able to maintain the q profile above 2 throughout the entire plasma [7]. Without the presence of a $q = 3/2$ surface in the plasma, the $3/2$ NTM does not go unstable. Steady-state high bootstrap fraction AT discharges in DIII-D are proposed to operate with this type of q profile and thus avoid the performance degradation associated with the $3/2$ NTM.

Another performance limiting instability that must be stabilized in all high performance AT discharges is the RWM. In the absence of a conducting wall surrounding the plasma, the beta is limited by an $n = 1$ external kink at a value of β_N (no wall). The presence of an ideal conducting wall immediately surrounding the plasma results

in a significantly higher beta limit, β_N (ideal). In the presence of a resistive wall, the $n = 1$ ideal kink is manifested as the RWM and can again grow. Like the ideal kink, the mode causes a significant loss of plasma thermal energy and leads to a disruption if unchecked. The parameter that measures the distance from the no-wall limit to the ideal wall limit is referred to as C_β and has a value of 0 at the no-wall limit and 1 at the ideal wall limit. Two techniques have been studied on DIII-D to address the RWM: wall stabilization by plasma rotation and active feedback control of the mode. Effective wall stabilization has been achieved by rotating the plasma with injected momentum from high power neutral beams while simultaneously reducing the magnetic error fields that produce magnetic drag and reduce the rotation speed [10]. When the rotation falls below a critical value, the RWM becomes unstable. In the wall stabilization experiments, the error correction was achieved using the set of six external picture frame coils (C-coil) on the vessel mid-plane (Fig. 2). By optimizing the error field correction, plasma rotation was maintained and it was demonstrated that the RWM can be stabilized up to twice the no-wall beta limit and to near the ideal wall limit.

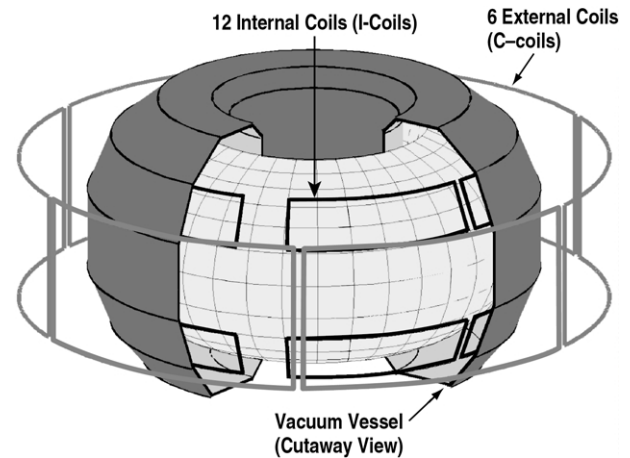


Fig. 2. Views of the two non-axisymmetric coil sets on DIII-D: the 6 external coils on the vessel midplane (C-coils) and the 12 internal coils (I-coils), 6 above and 6 below the midplane.

While wall stabilization due to plasma rotation is effective on DIII-D, devices with little or no momentum input may have insufficient rotation to stabilize the RWM. Calculations using the VALEN code show that without rotation, active feedback control of the RWM using magnetic fields generated by either internal or external sets of non-axisymmetric coils can effectively stabilize the mode significantly above the no-wall limit

even without rotation [24]. Experiments performed using reduced neutral beam torque to produce a slower rotating plasma clearly indicated the RWM was stabilized with the use of the external C-coils. As the gain of the feedback was reduced, the mode became progressively more unstable [12].

VALEN calculations predict, however, that the use of the external six-element C-coil can only stabilize the RWM up to values of $C_\beta \sim 0.5$, halfway between the no-wall and the ideal wall limit. To stabilize the mode up to near the ideal wall limit, requires an internal coil set. Such a set of internal coils (I-coil) has now been installed (Fig. 2) and is in routine use for RWM stabilization experiments as well as a variety of other experiments [25,26]. The I-coils consist of 12 separate coils (six above and six below the vessel midplane) mounted on the vessel surface and protected from the plasma by graphite armor tiles. Each coil consists of a single turn of a water-cooled copper conductor. The copper is insulated from the vessel with a high temperature polyimide, Vespel[®], and Kapton sheets (to increase tracking length) and was tested to 4 kV. The copper/insulator combination is isolated from the primary vacuum by being enclosed in a stainless steel tube that mounts directly to the vessel wall behind the graphite armor tiles. The coil leads are coaxial to eliminate any error fields and eliminate the net magnetic forces on the leads. The internal coil system offers a number of advantages relative to the external system: (1) the harmonic spectrum of the I-coils with their location above and below the midplane is better matched to the RWM ($m \sim 3-5$), (2) the closer proximity of the coils to the plasma allows a 7 kA single turn to produce $\sim 10\%$ more field at the plasma edge than the existing 20 kA-turn external C-coils, and (3) the location of the I-coils inside the conducting vessel eliminates the phase shift associated with the wall and produces a higher bandwidth coil system. The desire for the high bandwidth to permit stabilization of the high growth rates of the RWM near the ideal wall limit was further achieved with the low inductance coils ($\sim 4.5 \mu\text{H}$) and low inductance quadrupole cables ($\sim 20 \mu\text{H}$). The coils are powered by a set of switching power amplifiers with a switching frequency of 7 kHz and an effective bandwidth of a few hundred hertz. The new coil system is complemented by an extremely flexible patch panel that permits the coils and power supplies to be interconnected in a variety of different configurations that can produce a wide range of field harmonics. For the RWM stabilization experiments, the coils are typically hooked up as pairs of coils separated by 180° toroidally to produce an $n=1$ field pattern. Future experiments will be performed with amplifiers on each of the 12 coils to

permit simultaneous feedback control of both the $n=1$ and $n=2$ RWM.

Recent measurements have confirmed the engineering advantages of the internal coils relative to the external coil system. By optimizing the relative phasing of the upper coil set and the lower coil set to match the predicted structure of the ideal MHD external kink mode, the applied average magnetic field normal to the plasma surface was reduced to $\sim 20\%$ of that using the external coils [11]. This results in a stored magnetic energy of the I-coils that is less than 10% of the stored energy of the external coils.

Experimental results have also confirmed the improved stabilization that can be achieved using the internal coils [11]. Figure 3 indicates the effect of plasma rotation on RWM stability calculated using the MARS code [27]. Discharges to the right of the dotted line are stabilized by the plasma rotation relative to a surrounding conducting wall. As the rotation velocity drops below the critical value, the mode becomes unstable without active feedback. The curve labeled (a) shows the growth of the RWM at a relatively low value of C_β when the rotation velocity approaches the critical velocity for the case of no feedback. When active feedback using the C-coils is used, higher values of C_β are obtained [Fig. 3(b)], although some of the stabilization may be obtained from the finite plasma rotation. Despite a lower rotation speed, when the I-coils are used [Fig. 3(c)], a much higher value of $C_\beta \sim 0.7$ is obtained. In Fig. 3(d), the technique of

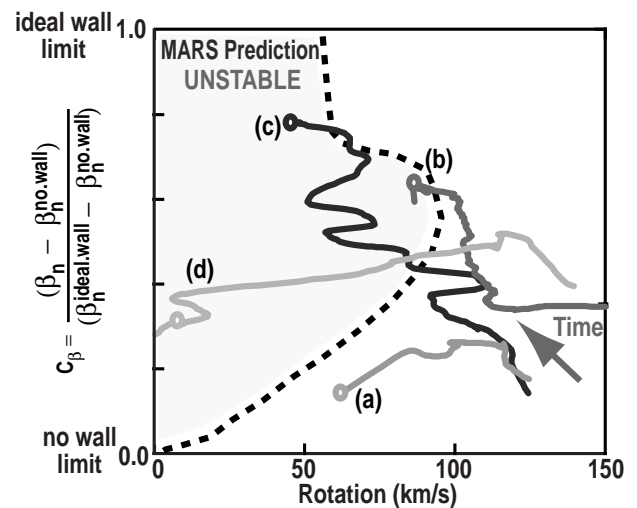


Fig. 3. Trajectories of discharges (a) without feedback, with feedback using (b) external and (c) internal coils, and (d) magnetic breaking with internal coil. The dotted line indicates the critical β calculated with MARS. The onset of the RWM is indicated by the open circle.

magnetic braking is used to slow the plasma rotation to zero outside the $q=2$ surface. Using the I-coils, the plasma was maintained stable for more than 100 ms (more than 20 times the resistive wall time constant). These results are consistent with separate measurements of the maximum growth rates of the RWM that each coil system has been able to stabilize. Maximum growth rates of the RWM observed with C-coil feedback have been $\sim 1000 \text{ s}^{-1}$, whereas almost twice the growth rate has been observed using the I-coils.

The early VALEN calculations assumed ideal amplifiers, i.e., infinite bandwidth and no latency between the command and the amplifier output voltage. In reality, the switching power amplifiers used in these experiments have considerable latency and a bandwidth well below 1 kHz. Recent VALEN calculations including the effects of finite bandwidth, noise, and total feedback system latency (including that introduced by supplies and the digital control system) have been performed and have provided guidance for a further upgrade to the power system that should permit reaching values of C_β above 0.9 with an unstabilized mode growth rate of 3000 s^{-1} . These calculations indicated that the present system of switching power amplifiers cannot meet those goals. Instead, a system consisting of commercial off-the-shelf audio amplifiers with low latency and bandwidth of 20 kHz is capable of reaching those goals with relatively low current and voltage requirements. The proposed upgrade will utilize a low inductance strip line ($< 1 \mu\text{H}$), audio amplifiers, and impedance matching transformers to achieve the predicted I,V requirements. To prevent the RWM from growing on a very slow time scale, the external coils using the existing switching power amplifiers will be used to provide stabilization in the DC to 20 Hz range.

A significant engineering problem for both ITER and any H-mode based Advanced Tokamak is the high impulsive and localized heat flux associated with the edge instability known as ELMs. Estimates for ITER based on the high predicted edge T_e pedestal ($\sim 4 \text{ keV}$) indicate that the large Type I ELMs will deposit approximately 20 MJ/ELM to the divertor region [28] with heat impulse product ($Qt^{-1/2}$) to the divertor plates as high as $185 \text{ MJ/m}^2 \text{ s}^{0.5}$ [29]. These levels will cause severe erosion to the graphite divertor target plates and decrease target lifetime below acceptable levels. Two approaches are being explored on DIII-D to address the issue of ELM control that will be a critical need in any reactor realization of an AT: the QDB [14,15] and the Stochastic Boundary [16]. In the first approach, counter NB injection is used to produce ELM-free high performance discharges

that contain the usual edge transport barrier characteristic of an H-mode and also an internal barrier that produces higher values of T_e and T_i than the standard H-mode. In both single null and balanced double null discharges, the high pulsed power loads associated with ELMs are replaced by a coherent MHD mode, referred to as the edge harmonic oscillation (EHO). The EHOs enhance particle transport through the plasma boundary resulting in good density and radiated power control and allow large temperature pedestals to be maintained, without the detrimental effects of large ELMs. Production of the QDB mode requires sufficient counter neutral beam injection, good divertor pumping, and a large plasma wall gap (10 cm) on the low field side. The mode has been obtained over the full range of triangularity ($0.16 < \delta < 0.82$) and safety factor ($3.4 < q_{95} < 5.8$) tested and the edge collisionality and beta span the projected ITER values. Values of $\beta_N H$ up to 7 have been maintained for $10 \tau_E$ and the mode has been maintained for 4 s or $35 \tau_E$ limited only by the neutral beam pulse duration. In initial studies, the peaked density and pressure profiles in these discharges led to lower beta limits, non-optimal bootstrap current profiles, and slow high-Z impurity accumulation in the core. However, localized profile control using ECH or ECCD has now been utilized to reduce the central high-Z impurity accumulation associated with the density peaking [30]. As a measure of the robust nature of the mode, it has been observed in JT-60U, ASDEX-Upgrade, and JET.

More recently a new technique of ELM suppression has been discovered using the new I-coils [16]. By alternating the current in adjacent coil section, an $n=3$ (120° periodicity) magnetic field structure is produced. Experiments were performed with the upper coil set in phase with the lower set (even parity) and out of phase (odd parity). In both cases, modification to the ELM character was seen, but significant suppression of the large Type I ELMs was obtained using the even parity (Fig. 4). In this configuration, large 70 Hz Type I ELMs are almost completely suppressed and are instead replaced with small 130 Hz oscillations with isolated ELM-like events. These isolated events, however, do not have the large stored energy dump on to the divertor target plates. Figure 5 shows the comparison of a standard H-mode discharge with Type I ELMs and one with the $n=3$ field pattern from the I-coil applied. The ELM suppression can readily be seen on the D_α light from the lower divertor [Fig. 5(c)]. Other characteristics of the ELM-suppressed discharges are that there is no degradation of the stored energy [Fig. 5(d)] and core radiated power is not increased [Fig. 5(e)]. The real significance of these

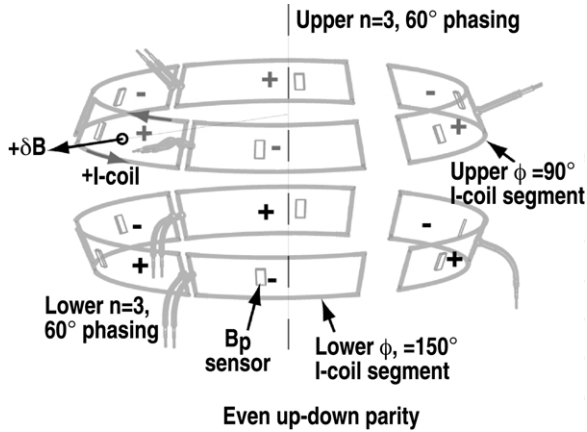


Fig. 4. An $n=3$ field configuration is produced by alternating the field and currents in each of the upper and lower I-coils. The upper and lower set of six coils can be either in phase (up/down “even” parity as shown in figure) or they can be out of phase (up/down “odd” parity).

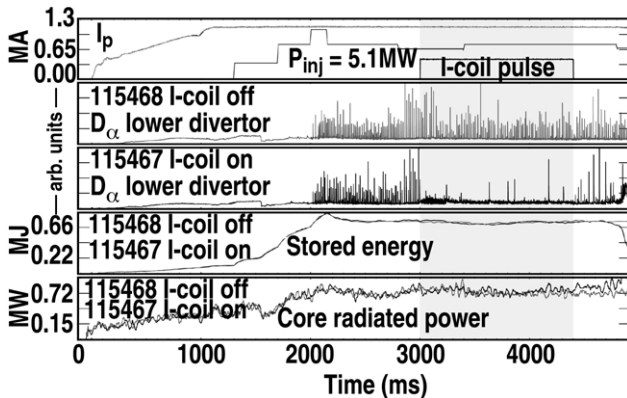


Fig. 5. Comparison of discharges 115648 (I-coil off) and 115667 (I-coil on). The I-coils were set up for up/down even parity. (a) The I-coil pulse is on from 3.0 to 4.5 s. (b) Large Type I are seen in 115648 with the I-coil off and (c) ELM suppression is seen in 115667 with the I-coils on. The stored energy (d) and radiated power (e) are unchanged between the two discharges.

discharges is that there is a factor of 20 reduction in the impulsive heat loading and the localized peaks in the divertor heat flux due to ELMs are reduced at least a factor of five. Field line tracing in the edge region indicates that the formation of small islands in the edge pedestal region may be responsible for the ELM suppression with a corresponding increase in the magnetic and density fluctuations in this region. In particular, the character of the edge profiles does not indicate any increase in stochasticity of the field lines because the pedestals in T_e , T_i , and n_e all remain of similar magnitude when the perturbing I-coil field is applied. In contrast, when the

odd parity configuration is applied, the edge pedestals all move inward; a behavior that is consistent with an edge that has become more stochastic. With this parity, the ELM frequency and amplitude are reduced with a corresponding increase in stochastic transport across the plasma boundary. This ELM suppression and modification technique using applied $n=3$ field perturbations represents an exciting new opportunity and possible solution to a serious engineering problem in next generation devices.

Earlier work demonstrated a good understanding of the ECCD process [31] with experimental verification of the modeling of both on-axis and off-axis ECCD needed for the AT discharges. In a demonstration of the progress toward a fully integrated AT discharge, off-axis ECCD was combined with NB current drive, RWM stabilization by NB induced rotation and error field reduction, and density control using in-vessel cryopumps. This integrated scenario resulted in a 100% non-inductively driven current discharge at high $\beta_N \sim 3$ for 2 s in a high triangularity, single null divertor [7]. Details of one of these high beta discharges are shown in Fig. 6. Prior to the application of the ECCD at 2.7 s, the majority of the

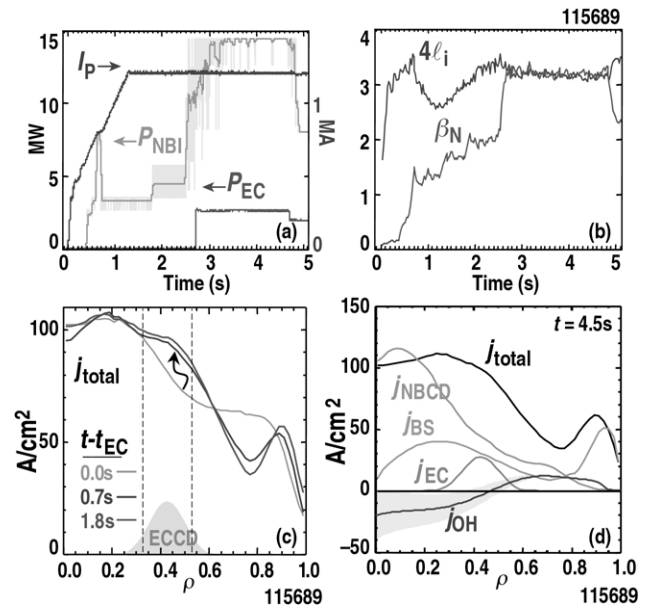


Fig. 6. A typical AT discharge with 100% non-inductive current, $\beta_N \sim 3.1$ and $\beta_T \sim 3.2\%$. (a) Plasma current I_p , neutral beam power P_{NBI} , EC power P_{EC} ; (b) Normalized beta, β_N , and the approximate no-wall beta limit, $4 \ell_i$; (c) significant current profile change observed at the time and location of the application of the EC pulse; (d) components of the non-inductive current at the end of the EC pulse.

inductively driven current is located at the mid-radius $\rho \sim 0.4-0.5$. The effect of the ECCD pulse applied off-axis to replace this current can clearly be seen in Fig. 6(c), where the total current increases at the location of the ECCD pulse. The various components of the total non-inductive current can be seen in Fig. 6(d) with the NBCD being responsible for most of the central current drive, the bootstrap current contributing $\sim 50\%$ of the total driven current, and EC supplying the remainder of the current. It can be seen that there is still a remnant inductive component near the axis that is in the opposite direction to the driven current because of the excess NBCD. Both simulation and experiments indicate that even in the absence of this excess NBCD, the plasma response to off-axis ECCD is a reduction of the on-axis current due to a back EMF. The resulting current profile with strong negative central magnetic shear can result in an internal transport barrier near the plasma center that yields a more peaked pressure profile. This peaked pressure profile has significantly lower beta limits and is thus to be avoided in steady state AT discharges.

One additional tool in the AT arsenal on DIII-D that can be used to counteract this effect and drive current on axis very efficiently is Fast Wave Current Drive (FWCD). In addition, FWCD has the added benefit of increasing T_e and the electron beta, both effects that increase the efficiency of off-axis ECCD. DIII-D has three FWCD systems that are presently operational [32]. One is capable of generating 2.0 MW at 60 MHz and the other two are capable of operation from 60 to 120 MHz with a present limit of 1.0 MW at 120 MHz. Each transmitter drives a four-element phased array antenna that is protected by Faraday shields that are $\sim 50\%$ optically opaque. The antenna on the 60 MHz system is presently limited to 2 s operation at full power, while the other two water cooled antennas are capable of 10 s operation at 2 MW. An upgraded, more ITER-like antenna is planned for the 60 MHz system and the other two are planned to be switched to a fixed frequency near 120 MHz with 2.0 MW capability because of the higher efficiency of electron current drive at that frequency.

A critical element to the success of the DIII-D Advanced Tokamak program is the ability to flexibly implement the many required control schemes with adequate speed. This is provided by the DIII-D digital plasma control system (PCS) that has recently been upgraded [8]. A block diagram of the new architecture is shown in Fig. 7. The previous 40 MHz, i860 based system has been replaced by a Myrinet-based [33] cluster of PCI Intel Xeon processors operating at 2.4–3.0 GHz, yielding a thirty-fold increase in processing speed depending on the

application. There are presently 13 processors running in parallel with 11 used for real time discharge control. The processors use a Linux-based operating system that has been customized for true real-time functionality with all hardware and software interrupts disabled during the plasma discharge. Our data acquisition needs have been met by replacing the previous CAMAC-based digitizers with PCI form digitizers from D-TACQ systems [34]. These are 16 bit, 32 channel units with 250 kHz sampling that supports low latency real-time data acquisition. The computers are connected by a 2.0 Gbit/s, Myrinet switched network. The high speed fiber-based network provides the capability for real-time communication with PCS processors in diagnostic systems located in remote locations of the laboratory. This has permitted the addition of 32 channels of motional Stark effect data for the real-time computation of the safety factor and for inclusion of data from the Electron Cyclotron Emission diagnostic for real-time feedback on electron temperature. The addition of ion temperature and toroidal rotation profile data from the charge exchange recombination system and electron temperature and density profiles from the Thomson Scattering system are planned.

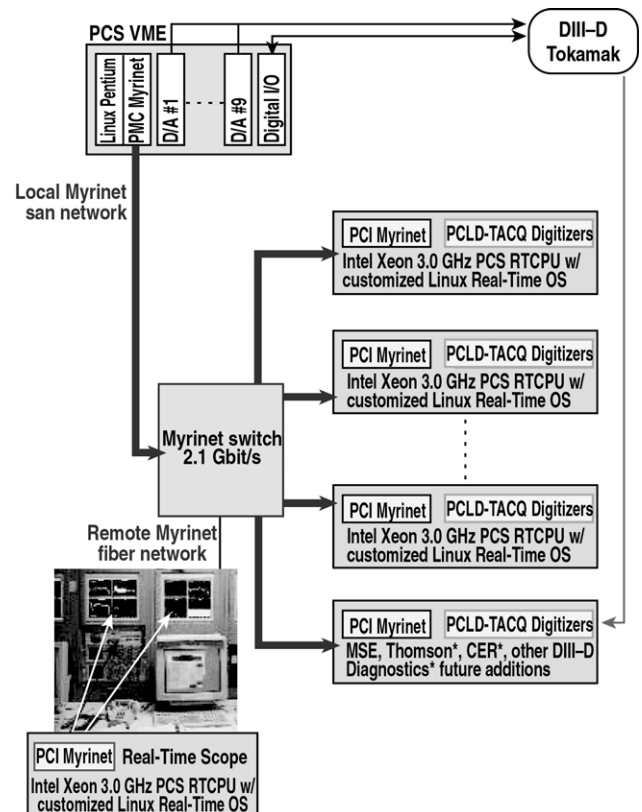


Fig. 7. Block diagram of the DIII-D plasma control system computer architecture.

The DIII-D PCS is one part of larger integrated plasma control approach that is utilized on DIII-D [35]. This refers to an approach to plasma control design that incorporates validated plasma/system models for design of control algorithms and makes extensive use of detailed simulations of the plasma, power supplies, and diagnostic systems to confirm controller performance. In addition to the PCS software itself, a suite of tools for applying this approach to plasma control design has been developed over the past decade. The tools include software for electromagnetic modeling, model validation, controller design and analysis, and offline simulation with both linear and non-linear models for plasma and hardware behavior. The DIII-D PCS software has presently been adapted for use on NSTX and MAST and is presently being developed for KSTAR and EAST.

III. FUTURE PLANS

A number of major system upgrades are planned for the period from April 2004 to March 2005. The most significant of these includes the increase in EC power and pulse length, the modification of the lower divertor for pumping highly triangular, double null divertors (DND), and the reversal of the injection direction of one of four neutral beam lines.

The EC upgrade involves the addition of three new 1 MW, 10 s, CPI gyrotrons for a total of 6 MW, 10 s generating capability. The two shorter pulse Gycom tubes will be held in reserve. In addition, a 1.5 MW, 10 s depressed collector tube developed by the US gyrotron program and built by CPI will be tested and utilized on DIII-D starting January 2005.

The lower divertor modification is motivated by the fact that EC driven current scales as $T_e/(n_e R)(\beta_e)^{1/2}$. Thus, in order to efficiently drive current, we need to provide effective pumping to reduce n_e in our target AT discharge shape. Theoretical modeling indicates that the beta limit increases sharply as plasmas are shaped more strongly, i.e., higher elongation and triangularity (Fig. 8) and this sharp increase is true for both β and β^* [2]. This effect is even stronger at broad pressure profiles [Fig. 8(a)] although the difference is somewhat smaller for β^* than for β . This prediction is confirmed by experiments in which the increased triangularity from our present pumped single null AT shape to our target double null shape resulted in a beta limit increase from $\beta_N \sim 3.6$ to 4.2 [Fig. 8(b)] [3]. These results indicate that optimized AT discharges require effective pumping in a high triangularity DND. Recent experiments have also indicated that while we can effectively pump $\sim 100\%$ of all the external particle input in our upper single null discharges, in the high triangularity DND shape, only $\sim 60\%$ of the

particle input can be pumped [36]. Our existing lower baffle [Fig. 9(a)] is located too far out to provide any pumping in the DND configuration. The proposed modification of the lower divertor will utilize the existing lower cryopump and extend the lower baffle across the vessel floor to match the outer strike point of the DND [Fig. 9(b)]. To provide experimental flexibility, the baffle will be designed to handle sufficiently high heat loads to serve as the target plate for either the outer strike point of the DND or both strike points of a single null configuration. The new configuration is also compatible with pumping an ITER shaped single null configuration [Fig. 9(c)].

The reversal of one of four neutral beam lines from the co- to the counter- direction will provide a tool to independently control power input and momentum input to the plasma (and thus rotation). The addition of this new control tool and the fact that some discharges will have no net momentum input will provide significant new capabilities for plasma control and physics studies. These include: (1) study of RWM feedback stabilization at low rotation, a condition more relevant to the proposed next generation experiments, (2) the lower rotation frequency

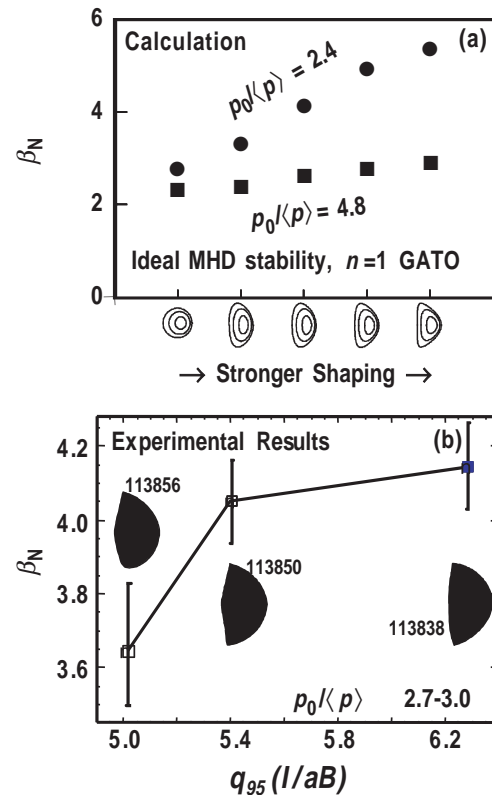


Fig. 8. Both theory (a) and experiment (b) show that β limits are maximized with strong shaping, characterized by an increasing "shape parameter" $S = q_{95} (I/aB) \sim a/R(1 + \kappa^2/2) [1 + 3/2(a/R)^2 \dots] f(\delta, \dots)$.

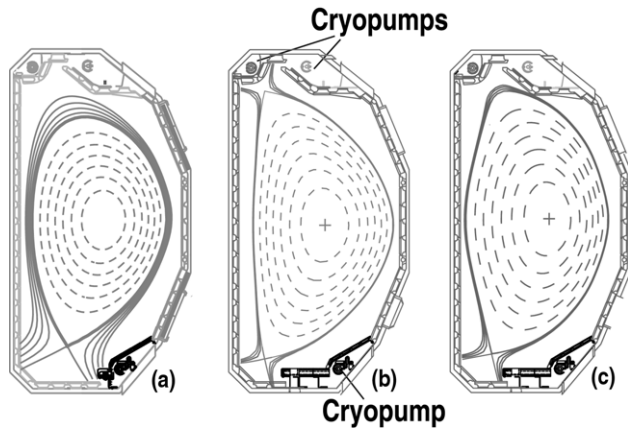


Fig. 9. (a) Existing lower divertor geometry showing existing cryopump under the conical lower outer baffle. (b) The new lower divertor geometry includes a flat baffle plate that extends from the conical baffle close to the outer strikepoint for the highly triangular double null divertor. (c) This new lower baffle geometry can also be used as the target plates for a lower single null configuration and for an ITER-shaped single null.

of the NTM should permit stabilization experiments with modulated ECCD, which may reduce the required EC power, (3) enhanced studies of the effect of rotation on the ELM-free quiescent H-mode, (4) understanding the physics of rotation, (5) enhanced transport barrier control by providing separate control of radial electric field and Shafranov shift, and (6) enable separate measurements of the radial electric field and current density from the MSE diagnostic.

IV. SUMMARY

Significant progress has been made in obtaining and sustaining enhanced performance discharges in DIII-D as a result of improved plasma control techniques. The six gyrotron EC system has provided current drive, heating, current and pressure profile control and stabilization of the NTM. The external control coils have reduced error fields and permitted high plasma rotation for RWM stabilization. A new highly efficient and flexible internal coil set has provided RWM stabilization and ELM suppression. The plasma control system upgrade provides higher computer power for real time diagnostics and sophisticated control algorithm. Planned upgrades to DIII-D systems include higher power EC, reversal of the injection direction of a neutral beam line for momentum control, and a new lower divertor for pumping high triangularity double null divertors.

ACKNOWLEDGMENT

Work supported by U.S. Department of Energy under Cooperative Agreement DE-FC02-04ER54698.

REFERENCES

- [1] P. N. YUSHMANOV, et al., "Scalings for Tokamak energy Confinement," *Nucl. Fusion* **30**, 1999 (1990).
- [2] A. D. TURNBULL, T. S. TAYLOR, M. S. CHU, et al., "Synergism Between Cross-Section and Profile Shaping in β Optimization of Tokamak Equilibria with Negative Central Shear," *Nucl. Fusion* **38**, 1467 (1988).
- [3] M. A. MAKOWSKI, T. A. CASPER, et al., "Effects of Profiles and Shape on Ideal Stability of Advanced Tokamak Equilibria," *Proc. 30th Euro. Conf. on Contr. Fusion and Plasma Phys.*, St. Petersburg, Russian Federation, 2003, ECA Vol. 27A, P-2.113, EPS (2003).
- [4] E. A. LAZARUS, L. L. LAO, et al., "An Optimization of Beta in the DIII-D Tokamak," *Phys. Fluids B* **4**, 3644 (1992).
- [5] J. LOHR, R. W. CALLIS, et al., "Performance of the 110 GHz System on the DIII-D Tokamak," T. K. MAU and J. DeGRASSIE, Eds., *Proc. 14th Top. Conf. on Radio Frequency Power in Plasmas*, Oxnard, California, 2001, p. 314, AIP (2001).
- [6] J. LOHR, et al., "Practical Experiences with the 6 Gyrotron System on the DIII-D Tokamak," *Proc. 20th IEEE/NPSS Symp. on Fusion Engin.*, San Diego, California, 2003, Institute of Electrical and Electronics Engineers, Inc., to be published.
- [7] C. M. GREENFIELD, et al., "Advanced Tokamak Research in DIII-D," *Proc. 31st Euro. Conf. on Plasma Phys. and Contr. Fusion*, London, United Kingdom, 2004, EPS (2004).
- [8] B. G. PENAFLOR, J. R. FERRON, et al., "Progress Toward Achieving Profile Control in the Recently Upgraded DIII-D Plasma Control System," *Proc. 23rd Symp. on Fusion Technol.*, Venice, Italy, 2004, to be published in *Fusion Engin. and Design*.
- [9] R. J. LaHAYE, D. A. HUMPHREYS, et al., "Stabilization of Neoclassical Tearing Modes by Active Control of Electron Cyclotron Current Drive Alignment in DIII-D," *Proc. 31st Euro. Conf. on Plasma Physics and Contr. Fusion*, London, United Kingdom, 2004.
- [10] A. M. GAROFOLO, T. H. JENSEN, L. C. JOHNSON, et al., "Sustained Rotational Stabilization of DIII-D Plasmas Above the No-Wall Beta Limit," *Phys. Plasmas* **9**, 1997 (2002).
- [11] M. OKABAYASHI, et al., "Control of the Resistive Wall Mode with Internal Coils in the DIII-D Tokamak," *Proc. 20th Int. Conf. on Fusion Energy*, Lisbon, Portugal, 2004.

- [12] A. M. GAROFALO, et al., "RWM Feedback Stabilization in DIII-D: Experiment-Theory Comparison and Implications for ITER," *Proc. 31st Euro. Conf. on Plasma Phys. and Contr. Fusion*, London, United Kingdom, 2004.
- [13] M. OKABAYASHI, et al., "Active Feedback Stabilization of the Resistive Wall Mode on the DIII-D Device," *Phys. Plasmas* **8**, 2071 (2001).
- [14] K. H. BURRELL, "Quiescent Double Barrier Mode in the DIII-D Tokamak," *Phys. Plasmas* **8**, 2153 (2001).
- [15] K. H. BURRELL, W. P. WEST, E. J. DOYLE, et al., "Edge Radial Electric Field Structure in Quiescent H-mode Plasmas in the DIII-D Tokamak," *Plasma Phys. Contr. Fusion* **46**, A165 (2004).
- [16] T. E. EVANS, et al., "Suppression of Large Edge Localized Modes in High Confinement DIII-D Plasmas with a Stochastic Magnetic Boundary," *16th Int. Conf. on Plasma Surface Interactions in Contr. Fusion Devices*, Portland, Maine, 2004.
- [17] D. G. WHYTE, et al., "Mitigation of Tokamak Disruptions Using High Pressure Gas Injection," *Phys. Rev. Lett.* **89**, 055001-1 (2002).
- [18] B. G. PENAFLO, et al., "Present Status of DIII-D Plasma Control System Computer Upgrades," *Proc. 4th IAEA Tech. Mtg. on Control, Data Acquisition and Remote Participation for Fusion Research*, San Diego, California, 2003, to be published in *Fusion Engin. and Design*.
- [19] Communications and Power Industries, Palo Alto, California.
- [20] Gycom, Nizhny Novgorod, Russia.
- [21] J. LOHR, S. W. DELAWARE, R. W. CALLIS, et al., "ECH Comes of Age for Magnetic Research," *Proc. 19th IEEE/NPSS Symp. on Fusion Engineering*, Atlantic City, New Jersey (Institute of Electrical and Electronics Engineers, Inc., Piscataway, New Jersey, 2002) p. 126
- [22] J. R. FERRON, et al., "Real Time Equilibrium Reconstruction for Control of the Discharge in the DIII-D Tokamak," *Proc. 24th Euro. Conf. on Contr. Fusion and Plasma Phys.*, Berchtesgaden, Germany, 1997, Vol. 21A, Part III, p. 1125, EPS (1998).
- [23] C. C. PETTY, R. J. La HAYE, T. C. LUCE, D. A. HUMPHREYS, et al., "Complete Suppression of the $m=2/n=1$ Neoclassical Tearing Mode Using Electron Cyclotron Current Drive on DIII-D," *Nucl. Fusion* **44**, 243 (2004).
- [24] J. BIALEK, A. H. BOOZER, M. E. MAUEL, G. A. NAVRATIL, "Modeling of Active Control of External Magnetohydrodynamic Instabilities," *Phys. Plasmas* **8**, 2170 (2001).
- [25] G. L. JACKSON, P. M. ANDERSON, et al., "Initial Results From the New Internal Magnetic Field Coils for Resistive Wall Mode Stabilization in the DIII-D Tokamak," *Proc. 30th Euro. Phys. Soc. Conf. on Contr. Fusion and Plasma Physics*, St. Petersburg, Russia, 2003.
- [26] P. M. ANDERSON, C. B. BAXI, A. G. KELLMAN, E. E. REIS, "Design, Fabrication, Installation, Testing and Initial Results of In-Vessel Control Coils for DIII-D," *Proc. 20th IEEE/NPSS Symp. On Fusion Engin.*, San Diego, California, 2003, Institute of Electrical and Electronics Engineers, Inc., Piscataway, to be published.
- [27] Y. Q. LIU, A. BONDESON, et al., *Phys. Plasmas* **7**, 3681 (2000).
- [28] A. LOARTE, G. SAIBENE, R. SASTORI, et al., "Characteristics of type I ELM energy and particle losses in existing devices and their extrapolation to ITER," *Plasma Phys. and Contr. Fusion* **45**, 1549 (2003).
- [29] A. W. LEONARD, A. HERMANN, K. ITAMI, et al., "The Impact of ELMS on the ITER Divertor," *J. Nucl. Mater.* **266-269**, 109 (1999).
- [30] E. J. DOYLE, T. A. CASPER, K. H. BURRELL, et al., "Core and Edge Aspects of Quiescent Double Barrier Operation on DIII-D with Relevance to Critical ITB Physics Issues," *Proc. 19th IAEA Fusion Energy Conf.*, Lyon, France, 2002, International Atomic Energy Agency, Vienna, (2002).
- [31] C. C. PETTY, R. PRATER, T. C. LUCE, R. A. ELLIS, et al., "Effects of Electron Trapping and Transport on Electron Cyclotron Current Drive on DIII-D," *Nucl. Fusion* **43**, 700 (2003).
- [32] R. I. PINSKER, F. W. BAITY, et al., "Fast Wave Antenna Loading in Advanced Tokamak Plasmas in DIII-D," *Proc. 31st Euro. Conf. on Plasma Phys. and Contr. Fusion*, London, United Kingdom, 2004.
- [33] Myricom, Inc. 325 N. Santa Anita Ave., Arcadia, California 91006.
- [34] D-TACQ Solutions Ltd., James Watt Bldg, Scottish Enterprise Tech. Park East Kilbride G75 0QD, Scotland, United Kingdom.
- [35] D. A. HUMPHREYS, J. R. FERRON, et al., "Integrated Plasma Control for Advanced Tokamaks," *Proc. 20th IEEE/NPSS Symp. On Fusion Engin.*, San Diego, California, 2003, O1B-1, Institute of Electrical and Electronics Engineers, Inc., Piscataway, 2003.
- [36] T. W. PETRIE, J. G. WATKINS, S. L. ALLEN, N. H. BROOKS, et al., "Changes in Particle Pumping Due to Variation in Magnetic Balance Near Double Null in DIII-D," *Proc. 30th Euro. Phys. Soc. Conf. on Contr. Fusion and Plasma Phys.*, St. Petersburg, Russia, 2003, ECA Vol. 27A, P-4.086, EPS, 2003, http://eps2003.ioffe.ru/PDFZ/P4_086.PDF.